Analysis of the Coverage of Tunable Matching Networks for the Imperfect Matching case

Eyad Arabi, *Member, IEEE,* Chris Gamlath, *Member, IEEE,* Kevin A. Morris, *Member, IEEE,* and Mark A. Beach, *Member, IEEE*

***Abstract*—Since conjugate (perfect) matching of complex loads and sources over a wide frequency band is not possible, imperfect matching is necessary. In this work, formulas for the coverage of tunable matching networks for imperfect matching have been derived for the first time. It has been found that the coverage area in this case expands beyond the perfect matching area with more circles required to define the coverage. Analytical expressions for the centers and radii of these circles have been derived for the first time. The theoretical analysis has been provided for the T and Π networks and verified by circuit simulation and measured data.**

***Index Terms*—Smith chart, tunable matching networks**

I. Introduction

THE fifth generation (5G) of mobile communications promises considerably higher data-rates as compared to the currently available fourth generation (4G) systems. The utilization of the spectrum below 6 GHz needs to be optimized to accommodate such high rates, which inevitably calls for tunable transceivers. A tunable matching network (MN) is at the heart of such tunable systems.

The primary design metric of tunable MNs, is the *coverage area*, which is defined as the set of all complex impedances that can be matched to a specific load (typically 50 Ω) when the tunable elements (variable capacitors) are swept across all combinations (the full dynamic range of the network). Since there are many different topologies of tunable MNs, it is important to have rigorous theoretical formulas to define and compare the coverage of these networks.

In [1]–[5], simulations have been used to define the coverage areas of tunable MNs. However, they do not indicate the limits of the tuning elements, and do not provide any physical insight about the networks. In [6], theoretical formulas have been presented; however, they provide the coverage for discrete impedance points (states) and do not give the continuous coverage. Even though the formulas in [7], [8] define the boundary area for the full dynamic range, they are presented for the complex rectangular plane, not the Smith chart (reflection coefficient plane). The power of the Smith chart as a visualization tool for the design and analysis of radio frequency (RF) systems is undoubted [9]. Therefore, in our previous works [10], [11], we have derived formulas for the coverage area on the Smith chart. These formulas, however, only define the coverage for the limited case of perfect matching (when the reflection coefficient is exactly zero), which is suitable only for narrowband matching. For practical applications requiring wideband operation (5G applications), imperfect matching must be considered [12]. Another example is power amplifiers where desired impedances are defined as load-pull contours. Since the optimal efficiency and output power contours are typically different, a compromise has to be made and a degree of mismatch is needed.

Manuscript received May 8th, 2018; revised July 5th, 2018; accepted July 25th, 2018. This work is supported by the British Engineering and Physical Sciences Research Council (EPSRC), under the FARAD project with grant number EP/M01360X/1 in collaboration with the University of Sheffield, Sheffield, UK.

The authors are with the department of Electrical and Electronic Engineering, University of Bristol, BS8 1UB, Bristol, UK. E-mail: {eyad.arabi, kevin.morris}@bristol.ac.uk

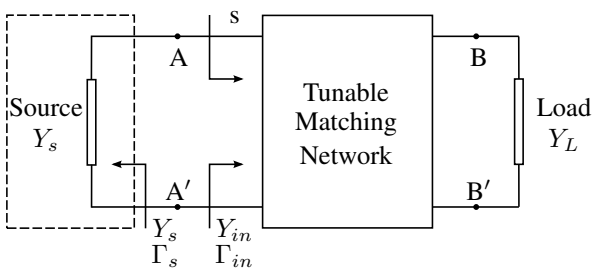

Fig. 1. Matching an arbitrary load to an arbitrary source with a tunable MN. Γ_{in} is the reflection coefficient when the source is not connected, while s is the power wave reflection coefficient when the source is connected.

In this work, we have extended the formulas of [10] to define the boundary area when the load is *imperfectly* matched to the source. Either the magnitude of the power wave reflection coefficient or the transducer power gain (G_T) can be used to specify the amount of mismatch between the source and load. The theoretical formulas presented here are compact; therefore, convenient for use in CAD tools and provide a useful instrument for the analysis of wideband tunable MNs.

II. Theory

The coverage of a tunable MN can be defined as the set of all complex impedances that can be *matched* to a specified load at a particular frequency. A typical scenario is illustrated in Fig. 1, where an arbitrary load is matched to an arbitrary source through a lossless network. In this work, the load is assumed to be real with the same value as the system impedance; however, the presented formulas can also be used for complex load matching if the reactive part of the load is absorbed by the MN.

If the admittance looking towards the input of the MN (Y_{in}) equals the conjugate of the admittance looking towards the source (Y_s^*), the source will be perfectly matched (also known

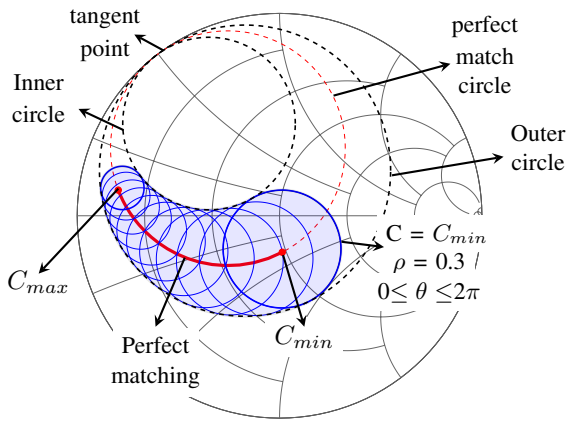

Fig. 2. The coverage area of a MN with a single tunable element. The perfect matching case correspond to the red solid line. The shaded area corresponds to imperfect matching with $\rho \leq 0.3$ (-5.2 dB). The blue circles correspond to different values of the tunable capacitor C. This graph is plotted with C_{min} = 0.2 pF and C_{max} = 10 pF.

as conjugate matching). The coverage of the tunable MN for this case has been analysed in our previous works [10], [11]. In this work, the coverage is defined as the set of all complex source impedances, which can be imperfectly matched to a resistive load with a specific transducer power gain (G_T). The analysis of [10] is, therefore, a special case with G_T = 1. The analysis is started by the power wave reflection coefficient (s) at plane A-A′, which is given by [13]

$$s = \rho\angle\theta = \frac{Z_s - Z_{in}^*}{Z_s + Z_{in}} = \frac{|Y_{in}|^2 - Y_{in}Y_s}{|Y_{in}|^2 + Y_{in}^*Y_s}, \tag{1}$$

where $(.)^*$ denotes the complex conjugate, ρ and θ are the magnitude and angle of the power wave reflection coefficient, respectively. $\rho \in (0,1) \subset \mathbb{R}$ corresponds to the the amount of mismatch, while $\theta \in (0, 2\pi) \subset \mathbb{R}$ is an arbitrary angle. It is worth mentioning that Γ_{in} and Γ_s in Fig. 1 are reflection coefficients (not power wave reflection coefficients) and are calculated as

$$\Gamma_{in/s} = \frac{Y_0 - Y_{in/s}}{Y_0 + Y_{in/s}}. \tag{2}$$

If the MN is lossless, the transducer power gain is

$$G_T = 1 - \rho^2. \tag{3}$$

To calculate the boundary for the imperfect matching case we need to find all the values of Y_s^* such that $|s|$ is less than or equal to a maximum limit ($\rho \leq \rho_{max}$). From equation (1), Y_s can be expressed as

$$Y_s = \frac{|Y_{in}|^2 (1 - s)}{Y_{in} + sY_{in}^*}, \qquad s = \rho\angle\theta. \tag{4}$$

Let us first consider the case where the MN has only one tunable element. If ρ is fixed and θ is allowed to take all values between 0 and 2π, an area will be defined for the coverage of the tunable MN as illustrated in Fig. 2. For each point within the perfect matching arc, there exists a circle which interior corresponds to $\rho \leq \rho_{max}$. Combining all the circles results

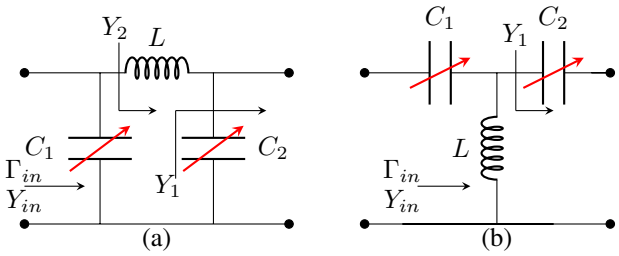

Fig. 3. Schematic of (a) Π network. (b) T network.

in the shaded area in Fig. 2, which is bounded by an *inner* and an *outer* circles as well as the C_{min} and C_{max} circles. Therefore, the boundary for imperfect matching can be defined theoretically by calculating the coordinates of the centers and radii of these circles. It is worth mentioning that the coverage in Fig. 2 and all other figures are based on Γ_s^* to compare with the perfect matching case.

A. Methodology for calculating the centers and radii of the inner and outer circles

As depicted in Fig. 2, the inner and outer circles as well as the perfect matching circle are all tanget to the $|\Gamma_s^*|$ = 1 circle at the same point. The problem of finding the centers and radii of these circles is, therefore, reduced to finding the tangent point and *any* other point and use the formula derived in [10] and given by

$$x_c = \frac{x_A\left(x_B^2 - x_A^2 + y_B^2 - y_A^2\right)}{2\left(-x_A^2 - y_A^2 + x_Ax_B + y_Ay_B\right)}, \tag{5a}$$

$$y_c = \frac{y_A\left(x_B^2 - x_A^2 + y_B^2 - y_A^2\right)}{2\left(-x_A^2 - y_A^2 + x_Ax_B + y_Ay_B\right)} \tag{5b}$$

and

$$R = \sqrt{(x_c - x_A)^2 + (y_c - y_A)^2}, \tag{5c}$$

where x_c and y_c are the coordinates of the center of the circle. R is the radius of the circle. x_A and y_A are the coordinates of the tangent point, and x_B and y_B are the coordinates of any other point in the circle.

The tangent point can be found as detailed in [10]. Unfortunately, finding the other arbitrary point is not as straightforward as the tangent point. In Fig. 4 (a), for the case of the Π network, the trajectory of Γ_s^* is traced for the case of θ = 0 and θ = π with C_2 swept and C_1 kept constant. These trajectories touch the outer and inner circles at P_1 and P_2, respectively. This tangency occurs only once at a critical value of C_2, which is referred to as C_2''. If this value is known, the coordinates of P_1 and P_2 can be calculated and the centers and radii of the inner and outer circles obtained from equation (5).

To calculate C_2'', the source impedance (Z_s^*) is expressed in terms of the input impedance (Z_{in}) for s = $\pm\rho$ (θ = 0 and π), which gives:

$$Z_s^* = \Re\{Z_{in}\}\frac{1 \pm \rho}{1 \mp \rho} + j\Im\{Z_{in}\}, \tag{6}$$

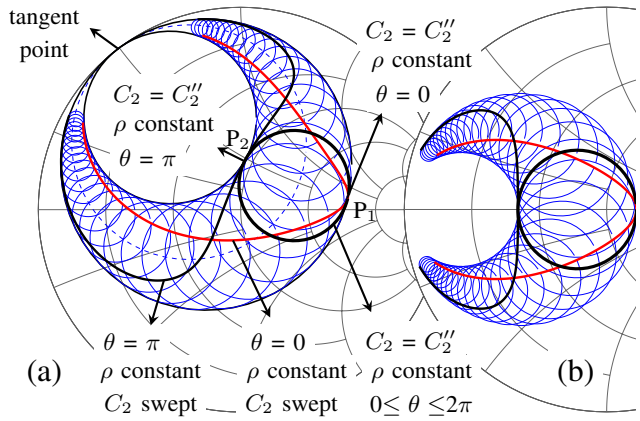

Fig. 4. Trajectory of Γ_s^* for θ = 0 and $\theta = \pi$ for the Π network of Fig. 3 (a). (a) C_2 is swept between -20 pF and 20 pF (blue circles). ρ, the frequency, C_1, and L are kept constant. (b) Same as (a) but with C_1 swept and C_2 constant.

where $\Re\{.\}$ and $\Im\{.\}$ denote the real and imaginary, respectively. It can be inferred from (6) that the transformation form Z_{in} to Z_s^*, which is a bilinear transformation, affects the real part only since the imaginary part of Z_s^* is the same as that of Z_{in}. It can be deduced, focusing on the real part , that P_1 and P_2 are stationary points; therefore, C_2'' can be calculated by solving

$$\frac{\partial \Re\{Z_{in}\}}{\partial C_2} = 0. \tag{7}$$

For the case of sweeping C_1 (Fig. 4 (b)), C_1'' can be calculated similarly by substituting C_1 for C_2 in equation (7).

The analysis method presented in this section can be applied to any lossless network with ideal lumped components or transmission lines. The Π and T networks are analyzed in the following sections, respectively to illustrate the method.

B. Analysis of Π*-type Networks*

The schematic of a Π network is illustrated in Fig. 3 (a). Firstly, C_1 is swept while C_2 is held constant at either its minimum or maximum to obtain the first pair of circles. Secondly, C_2 is swept while C_1 is held constant to get the second pair of circles. If

$$C_{min} < C_2' < C_{max}, \tag{8}$$

where

$$C_2' = \frac{1}{\omega^2 L}, \tag{9}$$

an auxiliary circle is needed to complete the boundary [10].

1) C_1 variable and C_2 constant: For the first case, $C_2 \in \{C_{min}, C_{max}\}$ while C_1 can take any real number between these two limits. To plot the complete circle, however, we will let $C_1 \in \mathbb{R}$. The first point to be calculated is the point at which this circle is tangent to the outer circle ($|\Gamma_s^*| = 1$). This point is referred to as point A and corresponds to $C_1 = \infty$. Using this value, the real and imaginary parts of Γ_s^* are

$$x_A = -1 \tag{10a}$$

and

$$y_A = 0, \tag{10b}$$

respectively. To obtain the other arbitrary point equation (7) gives

$$C_1'' = \frac{Y_0^2 L - C_2\left(1 - \omega^2 L C_2\right)}{\left(1 - \omega^2 L C_2\right)^2 + \left(Y_0 \omega L\right)^2}, \tag{11}$$

where Y_0 is the characteristic and load admittance, L is the inductance and ω is the angular frequency. Using this value for C_1 the real and imaginary parts of Y_{in} are calculated as

$$\Re\{Y_{in}\} = \frac{Y_0\left(1 - \omega^2 C_2 L\right) + Y_0 \omega^2 C_2 L}{\left(1 - \omega^2 C_2 L\right)^2 + \left(Y_0 \omega L\right)^2} \tag{12a}$$

and

$$\Im\{Y_{in}\} = \frac{\omega C_2\left(1 - \omega^2 C_2 L\right) - Y_0^2 \omega L}{\left(1 - \omega^2 C_2 L\right)^2 + \left(Y_0 \omega L\right)^2} + \omega C_1'', \tag{12b}$$

from which the real and imaginary parts of Y_s can be calculated as

$$\Re\{Y_s\} = \frac{|Y_{in}|^2 \Re\{Y_{in}\}\left(1 - \rho^2\right)}{\left[\Re\{Y_{in}\}\left(1 \pm \rho\right)\right]^2 + \left[\Im\{Y_{in}\}\left(1 \mp \rho\right)\right]^2} \tag{13a}$$

and

$$\Im\{Y_s\} = \frac{|Y_{in}|^2 \Im\{Y_{in}\}\left(1 \mp \rho\right)^2}{\left[\Re\{Y_{in}\}\left(1 \pm \rho\right)\right]^2 + \left[\Im\{Y_{in}\}\left(1 \mp \rho\right)\right]^2}, \tag{13b}$$

where the upper of the ($\pm$ and $\mp$) refers to the case where θ = 0, while the lower refers to the case where $\theta = \pi$. These two cases correspond to the outer and inner circles, respectively. Finally, the real and imaginary parts of Γ_s^* can be calculated as

$$x_B = \frac{Y_0^2 - \Re\{Y_s\}^2 - \Im\{Y_s\}^2}{\left(Y_0 + \Re\{Y_s\}\right)^2 + \Im\{Y_s\}^2} \tag{14a}$$

and

$$y_B = \frac{-2 Y_0 \Im\{Y_s\}}{\left(Y_0 + \Re\{Y_s\}\right)^2 + \Im\{Y_s\}^2}. \tag{14b}$$

Once the coordinates of the two points A and B are calculated, the centers and radii of the inner and outer circles can be calculated from equation (5).

2) C_2 variable and C_1 constant: For the tangent point of this case, C_2 is assigned a value of ∞, which yields

$$Y_s = jB_s, \tag{15a}$$

where

$$B_s = \frac{\omega^2 L C_1 - 1}{\omega L}, \tag{15b}$$

from which the coordinates of Γ_s^* can be calculated directly using (14). For the case of the other point, solving (7) yields

$$C_2'' = \frac{C_1}{\omega^2 L C_1 - 1}, \tag{16}$$

which can be used to calculate the real and imaginary parts of Y_{in} from equation (12) by replacing C_2 and C_1'' with C_2'' and

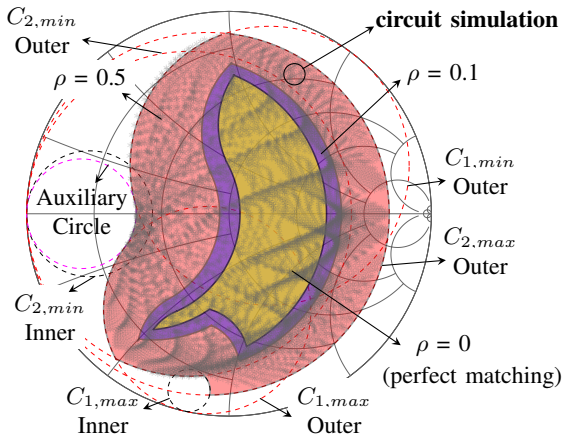

Fig. 5. Simulation results of the Π network of Fig. 3 (a). L = 12 nH, C_{min} = 2 pF, C_{max} = 10 pF, frequency = 0.7 GHz, ρ = 0, 0.1, and 0.5. Full circles and circuit simulation are included for the case of ρ = 0.5.

C_1, respectively. Next, (13) and (14) can be used to calculate Y_s and the coordinates of Γ_s^*, respectively.

Once the centers and radii of the inner and outer circles are calculated, the complete coverage can be plotted as illustrated in Fig. 5 for the perfect matching case as well as ρ = 0.1 and 0.5. To verify the theory, circuit simulation has also been included for ρ = 0.5. As expected, increasing ρ expands the coverage at the cost of a higher return loss.

C. Analysis of T-type Networks

The schematic of the T network is illustrated in Fig. 3 (b). The analysis of this network is similar to the Π network.

1) C_1 variable and C_2 constant: For this case $C_2 \in \{C_{min}, C_{max}\}$ while $C_1 \in \mathbb{R}$. To calculate the tangent point (point A), C_1 is assigned a value of zero leading to zero values of Y_{in} and Y_s. Therefore, the real and imaginary parts of Γ_s^* are

$$x_{A1} = 1 \tag{17a}$$

and

$$y_{A1} = 0, \tag{17b}$$

respectively. To calculate the coordinates of the second point (point B) equation (7) cannot be used because the partial derivative of $\Re\{Z_{in}\}$ with respect to C_1 is zero. Sweeping C_1 does not affect $\Re\{Z_{in}\}$ and hence the trajectories of Γ_s^* for θ = 0 and θ = π are identical to the inner and outer circles, respectively as illustrated in Fig. 6. Therefore, in this particular case, the choice of C_1 is arbitrary. A logical choice is C_1 = ∞, based on which the real and imaginary of Y_{in} are given by

$$\Re\{Y_{in}\} = \frac{Y_0\left(\omega C_2\right)^2}{Y_0^2 + \left(\omega C_2\right)^2} \tag{18a}$$

and

$$\Im\{Y_{in}\} = \frac{Y_0^2 \omega C_2}{Y_0^2 + \left(\omega C_2\right)^2} - \frac{1}{\omega L}, \tag{18b}$$

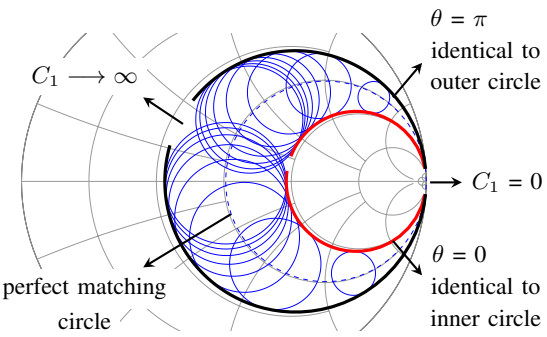

Fig. 6. Trajectory of Γ_s^* for θ = 0 and θ = π for the T network of Fig. 3 (b). C_1 is swept (blue circles correspond to different values of C_1). ρ, the frequency, C_2, and L are kept constant.

respectively. These values can be used in equations (13) (a) and (13) (b) to calculate the values of Y_s, which are subsequently used in equation (14) to calculate the coordinates of Γ_s^* for the two cases where $\theta \in \{0,\pi\}$.

2) C_2 variable and C_1 constant: For this case $C_1 \in \{C_{min}, C_{max}\}$ while $C_2 \in \mathbb{R}$. The tangent point in this case corresponds to C_2 = 0, which gives

$$Y_{in} = jB_s, \tag{19a}$$

where

$$B_s = \frac{\omega C_1}{1 - \omega^2 C_1 L}. \tag{19b}$$

Y_s can be calculated from (13) as

$$Y_s = jB_s, \tag{20}$$

which is used in (14) to calculate the coordinates of Γ_s^*.

For the case of the second point, solving equation (7) gives

$$C_2'' = \frac{1}{\omega^2 L}. \tag{21}$$

The real and imaginary parts of Y_{in} can be calculated receptively as

$$\Re\{Y_{in}\} = \frac{\Re\{Y_2\}\left(\omega C_1\right)^2}{\left(\Re\{Y_2\}\right)^2 + \left(\Im\{Y_2\} + \omega C_1\right)^2} \tag{22a}$$

and

$$\Im\{Y_{in}\} = \frac{\omega C_1\left[\left(\Re\{Y_2\}\right)^2 + \left(\Im\{Y_2\}\right)^2 + \Im\{Y_2\}\omega C_1\right]}{\left(\Re\{Y_2\}\right)^2 + \left(\Im\{Y_2\} + \omega C_1\right)^2}, \tag{22b}$$

where

$$\Re\{Y_2\} = \frac{Y_0\left(\omega C_2''\right)^2}{Y_0^2 + \left(\omega C_2''\right)^2} \tag{22c}$$

and

$$\Im\{Y_2\} = \frac{Y_0^2 \omega C_2''}{Y_0^2 + \left(\omega C_2''\right)^2} - \frac{1}{\omega L}. \tag{22d}$$

Next, equations (13) and (14) can be used to calculate the coordinates of Y_s and Γ_s^*, respectively. Once the coordinates

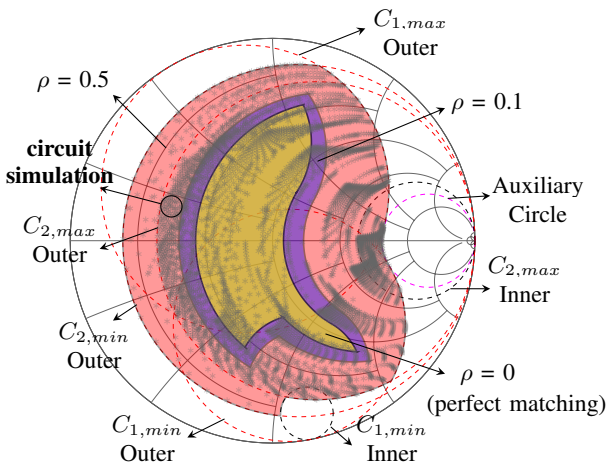

Fig. 7. Simulation results of the T network of Fig. 3 (b). L = 12 nH, C_{min} = 2 pF, C_{max} = 10 pF, frequency = 0.7 GHz, ρ = 0, 0.1, and 0.5. Full circles and circuit simulation are presented for the case of ρ = 0.5.

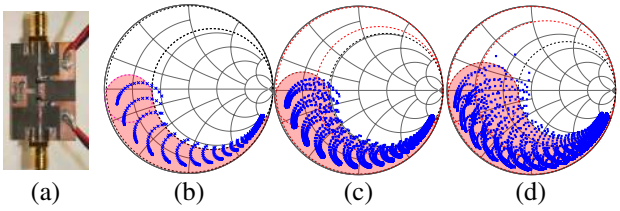

Fig. 8. Measurement and theory for a T network. (a) Photograph of the fabricated circuit. (b) ρ = 0 (Perfect matching). (c) ρ = 0.1 (-10 dB), G_T = -0.04 dB. (d) ρ = 0.3 (-5 dB), G_T = -0.4 dB. The measurement is performed at 0.5 GHz with: C_{min} = 1 pF, C_{max} = 9 pF and L = 10 nH.

of Γ_s^* are known, equation (5) can be used to calculate the centers and radii of the circles for this case.

In Fig. 7 the complete coverage of the T network is illustrated for the perfect matching case as well as ρ = 0.1 and ρ = 0.5. For the latter case, circuit simulations have also been included to verify the theory.

III. Measured Results

A prototype T network has been fabricated as depicted in Fig. 8 (a) to verify the theoretical formulas derived in the previous sections. Lumped components have been used for the fixed elements while varactors (Infineon BB388) have been used for the tunable capacitors. The physical size of the circuit has been miniaturized and the measurements have been taken at a relatively low frequency (0.5 GHz) to reduce the electrical size. With a load of 50 Ω, Γ_{in} is measured directly with a vector network analyzer (Keysight N5242A). The connectors and feed structures have been de-embedded. Γ_s^* is calculated directly from Y_s, which is calculated from equation (4). To compare the theory and measurement, the varactor has been characterized separately to determine its minimum and maximum capacitance values.

The measured results compared to the theoretical coverage are illustrated in Fig. 8 (b)-(d) for three different values of ρ. It can be observed that a good agreement between the simulation and the measurement has been achieved. The minor discrepancies can be attributed to the losses and parasitics of the inductors and capacitors used in the prototype. As discussed in [10], any impedance on the edge of the Smith chart has either a zero or infinite real part. To match such impedance to a real load, the MN must be lossless. For the case of practical MNs with non-zero losses, the coverage shifts towards the point of infinity impedance (middle right of the chart), which is evident in Fig. 8.

IV. Conclusion

The theoretical analysis of the coverage of tunable MNs, which is presented in our previous work, has been extended to include the coverage when the load is not perfectly matched to the source. We believe the formulas in this work provide a powerful tool for the analysis of tunable MNs. As a future work, this analysis can be extended by including the losses of the MN to provide a more general design tool for tunable MNs.

References

[1] C. Sanchez-Perez, J. de Mingo, P. L. Carro, and P. Garcia-Ducar, "Design and Applications of a 300 - 800 MHz Tunable Matching Network," *IEEE J. Emerg. Sel. Topics Circuits Syst.*, vol. 3, no, 4, pp. 531–540, Dec 2013.

[2] V. Freitas, J.-D. Arnould, and P. Ferrari, "General expression for tunable matching network efficiency in the case of complex impedances," *Microw. Opt. Technol. Lett.*, vol. 57, no. 5, pp. 1160–1166, 2015.

[3] C. Hoarau, N. Corrao, J. D. Arnould, P. Ferrari, and P. Xavier, "Complete Design and Measurement Methodology for a Tunable RF Impedance-Matching Network," *IEEE Trans. Microw. Theory Techn.*, vol. 56, no. 11, pp. 2620–2627, Nov 2008.

[4] F. C. W. Po, E. de Foucauld, D. Morche, P. Vincent, and E. Kerherve, "A Novel Method for Synthesizing an Automatic Matching Network and Its Control Unit," *IEEE Trans. Circuits and Syst. I, Reg. Papers*, vol. 58, no. 9, pp. 2225–2236, Sept 2011.

[5] M. Schmidt, E. Lourandakis, A. Leidl, S. Seitz, and R. Weigel, "A comparison of tunable ferroelectric Π- and T-matching networks," in *Proc. Eur. Microw. Conf.*, pp. 98–101, Oct 2007.

[6] P. Sjblom and H. Sjland, "Constant Mismatch Loss Boundary Circles and Their Application to Optimum State Distribution in Adaptive Matching Networks," *IEEE Trans. Circuits Syst. II, Exp. Briefs*, vol. 61, no. 12, pp. 922–926, Dec 2014.

[7] M. Thompson and J. K. Fidler, "Determination of the impedance matching domain of impedance matching networks," *IEEE Trans. Circuits Syst. I, Reg. Papers*, vol. 51, no. 10, pp. 2098–2106, Oct 2004.

[8] Y. Sun and J. Fidler, "Determination of the impedance matching domain of passive {LC} ladder networks: Theory and implementation," *J. Franklin Inst.*, vol. 333, no. 2, pp. 141 – 155, 1996.

[9] T. Lee, "The Smith Chart Comes Home [President's Column]," *IEEE Microw. Mag.*, vol. 16, no. 10, pp. 10–25, Nov 2015.

[10] E. Arabi, K. A. Morris, and M. A. Beach, "Analytical Formulas for the Coverage of Tunable Matching Networks for Reconfigurable Applications," *IEEE Trans. Microw. Theory Techn.*, vol. 65, no. 9, pp. 3211–3220, Sept 2017.

[11] E. Arabi, X. Jiao, K. Morris, and M. Beach, "Analysis of the coverage of tunable matching networks with three tunable elements," in *IEEE MTT-S Int. Microw. Symp. Dig.*, Honolulu, HI, USA, Jun. 2017, pp. 904–906.

[12] R. Fano, "Theoretical limitations on the broadband matching of arbitrary impedances," *J. Franklin Inst.*, vol. 249, no. 1, pp. 57 – 83, 1950.

[13] K. Kurokawa, "Power Waves and the Scattering Matrix," *IEEE Trans. Microw. Theory Techn.*, vol. 13, no. 2, pp. 194–202, Mar 1965.